POLITECNICO DI TORINO
Repository ISTITUZIONALE

Discretization error estimation for EUDEMO plasmaedge simulations using SOLPSITER with fluid neutrals

Original
Discretization error estimation for EUDEMO plasmaedge simulations using SOLPSITER with fluid neutrals / Van Uytven, W., Dekeyser, W., Subba, F., Wiesen, S., Horsten, N., Vervloesem, N., Baelmans, M.. - In: CONTRIBUTIONS TO PLASMA PHYSICS. - ISSN 0863-1042. - 64:7-8(2024). [10.1002/ctpp.202300125]

Availability:
This version is available at: 11583/2997575 since: 2025-02-18T12:37:44Z

Publisher:
John Wiley and Sons Inc

Published
DOI:10.1002/ctpp.202300125

Terms of use:

This article is made available under terms and conditions as specified in the corresponding bibliographic description in the repository

Publisher copyright
Wiley postprint/Author's Accepted Manuscript

This is the peer reviewed version of the above quoted article, which has been published in final form at http://dx.doi.org/10.1002/ctpp.202300125.This article may be used for non-commercial purposes in accordance with Wiley Terms and Conditions for Use of Self-Archived Versions.

(Article begins on next page)

09 November 2026

Discretization error estimation for EU-DEMO plasma-edge simulations using SOLPS-ITER with fluid neutrals

Wim Van Uytven[a,*], Wouter Dekeyser[a], Fabio Subba[b], Sven Wiesen[c], Niels Horsten[a], Sander Van den Kerkhof[a], Nathan Vervloesem[a], Martine Baelmans[a]

[a] *KU Leuven, Department of Mechanical Engineering, Celestijnenlaan 300A, 3001 Leuven, Belgium*
[b] *NEMO Group, Politecnico di Torino, Italy*
[c] *Forschungszentrum Jülich GmbH, Institut für Klima- und Energieforschung - Plasmaphysik, 52425 Jülich, Germany*

Abstract

Keywords: discretization error, plasma-edge modeling, SOLPS-ITER, EU-DEMO, fluid neutral atoms

1. Introduction

Plasma boundary codes are used to study the particle and power exhaust challenges in magnetic confinement fusion devices. SOLPS-ITER [1, 2] is currently the most widely used one of these codes. It is used to help interpret exhaust scenarios in existing devices, and to make predictions and design decisions for future fusion devices such as ITER [3] and (EU-) DEMO [4, 5, 6].

The two main physics modules of SOLPS-ITER are B2.5 and EIRENE. B2.5 is a finite volume code to solve the Branskii equations for the plasma [7]. EIRENE is a particle tracing kinetic Monte Carlo code, used to simulate the neutral particles in the plasma edge [8].

Many different factors can contribute to differences between the simulation results and physical reality. These factors can be grouped in two main categories: model errors and numerical errors. The model errors are the differences between the equations which the code aims to solve, and reality. Examples of possible model errors in SOLPS-ITER are the assumption of perfect fluid behavior of the plasma, the lack of a self-consistent description of plasma turbulence, uncertainties on the atomic and molecular reaction databases, the assumption of perfect toroidal symmetry, etc. The numerical errors on the other hand encompass the differences between the obtained simulation result, and exact solution of the equations which the code aims to solve.

Simulation times for plasma boundary codes are notoriously long, especially when coupling to kinetic neutrals and/or including electromagnetic drifts. DEMO simulations

*Corresponding author
Email address: wim.vanuytven@kuleuven.be (Wim Van Uytven)

with drifts and kinetic neutrals can take weeks to months to converge. To keep the simulation time from becoming unmanageable, quite coarse B2.5 grids are typically used.

K. Ghoos et al. [9] showed, however, that for a partially detached ITER case, the discretization error for the peak heat flux was about 63 % on a 74×28 grid (meaning 74 cells in the poloidal direction, and 28 cells in the radial direction), which is unacceptable. Subsequent grid refinement led to an estimated discretization error of 23 % for a 148×56 grid and 11 % for a 296×112 grid.

The three earlier cited EU-DEMO modeling efforts in SOLPS-ITER ([4, 6, 5]) all employ a 96×36 B2.5 mesh. Since the physical size of EU-DEMO is even larger than that of ITER, a significant discretization error could be expected as well.

This paper presents a first step in an effort to quantify the numerical errors of (EU-) DEMO simulations with SOLPS-ITER, and subsequently to be able to find an optimal balance between computational cost and numerical accuracy. This first step focuses fully on the discretization error, of which the importance was highlighted above.

Here, we employ a fluid neutral model in B2.5 instead of the EIRENE kinetic neutral Monte Carlo code. This brings two advantages. First, there is no risk that the estimates of the discretization error are contaminated by remaining statistical errors from the Monte Carlo noise. Second, we can add a "very fine" grid with a resolution of 384×144, which would be computationally infeasible in combination with kinetic neutrals.

2. Numerical errors in SOLPS-ITER

For SOLPS-ITER simulations with kinetic neutrals, the total numerical error, ϵ_{num}, can be written as

$$\epsilon_{\text{num}} = \epsilon_{\text{s}} + \epsilon_{\text{b}} + \epsilon_{\text{d}} + \epsilon_{\text{c}}. \tag{1}$$

ϵ_{s} is the statistical error, following directly from the Monte Carlo noise of the kinetic neutral solver EIRENE. The finite sampling bias error, ϵ_{b}, is a deterministic error which arises due to the coupling of the statistical noise with the non-linear plasma model. Both ϵ_{s} and ϵ_{b} are zero when using fluid neutrals instead of EIRENE.

ϵ_{d} and ϵ_{c} are the dicretization and convergence error, respectively. They are explained in the following subsections.

2.1. Discretization error

The discretiztaion error, ϵ_{d}, follows from the finite resolution of the finite volume mesh. The evolution of the discretization error is described by Richardson extrapolation [10], which assumes that ϵ_{d} scales with $h^{p_{\text{d}}}$, where h is a measure for the grid spacing, and p_{d} is the order of convergence of the employed numerical schemes. It then follows that

$$\Phi_0 \approx \Phi_h + \frac{\Phi_h - \Phi_{rh}}{r^{p_{\text{d}}} - 1}, \tag{2}$$

where r is the refinement factor between subsequent grids, Φ_h is a solution at a certain location on the finest grid, Φ_{rh} is the solution at the same location on the second-finest

grid, and Φ_0 is the extrapolated estimate for the solution on an infinitely fine grid. The estimated discretization error on the finest grid is thus

$$\epsilon_{\mathrm{d},h} = \Phi_0 - \Phi_h \approx \frac{\Phi_h - \Phi_{rh}}{r^{p_\mathrm{d}} - 1}, \tag{3}$$

and similarly for the other grids.

When three sequentially refined grids are available, the order of convergence can be estimated as

$$p_\mathrm{d} \approx \frac{\log(\frac{\Phi_{rh} - \Phi_{r^2h}}{\Phi_h - \Phi_{rh}})}{\log(r)}. \tag{4}$$

The estimates of ϵ_d and p_d are only reliable if the cases are close to grid convergence. The B2.5 code employs a mixture of first-order upwind schemes, and second-order central schemes. Linear interpolation is used to determine vertex and cell face values based on cell-centered information. Hence, the expected order of convergence lies between 1 and 2. In practice, determining p_d according to Eq. 4 was found to be unreliable in Ref. [9]. In Section 4.2 it is shown that the same problem is present here. We hypothesize that this is due to the complex nature of plasma boundary simulations, containing many non-linear transport and sink/source terms. It is then advised to be conservative and use $p_\mathrm{d} = 1$ for the estimates of ϵ_d. As was done in Refs. [9] and [11], we also apply a safety factor of 1.25 to the estimates of the discretiztaion errors, as suggest by Roache [12].

2.2. Convergence error

The convergence error, ϵ_c, is the remaining imbalance in the discretized conservation equations. When using fluid neutrals instead of Monte Carlo kinetic neutrals, it is possible to converge SOLPS-ITER simulations to machine accuracy, thereby reducing the convergence error to practically zero (or at least many orders of magnitude lower than any other error contribution). This is, however, not strictly necessary for correct interpretation of results, and using a less strict convergence criterion can save a significant amount of computational time for the most demanding cases (multi-species + fine grids). Instead, we consider a simulation to be converged if all default time traces (ion and electron temperature and electron density at inner and outer strikepoint, and at the outermost cell of the outer midplane) change less than 0.05% over the last 1000 iterations. An additional criterion is that all residuals are decreasing monotonically. The convergence error is then negligible compared to the estimated discretization errors.

3. Simulation setup

This section describes the set-up of the simulations and the different B2.5 meshes used for the grid convergence study. To increase the generality of the study, we test five different cases: three with only deuterium, and two with deuterium, helium, and argon, including all ionization stages. For the deuterium atoms, we use the so-called advanced fluid neutral model [13, 14], which gives improved agreement with EIRENE compared to the default fluid neutral models in SOLPS-ITER. We use the new extended grids version

of the SOLPS-ITER code [15]. It was shown in Ref. [14] that the improved discretization in this new extend grids version of the code is essential for the accuracy of fluid neutral models. The helium and argon neutrals are still described by the standard fluid neutral model [16]. The plasma model is simplified by turning off the electromagnetic drifts and currents. This allows to use a larger timestep (10^{-4} s was used for most cases, while simulations with drifts typically require dropping the timestep to 10^{-6} s or lower), which is essential to get a solution on the finest grid in reasonable time.

3.1. Computational meshes

Although the new SOLPS-ITER code can technically simulate up to the real vessel walls, grid generation and code convergence are still challenging for these so-called fully extended grids. Therefore, we still employ a standard "narrow" grid, where the radial extent of the plasma grid stops at the first intersection with the wall. We start from the same 96×36 grid which was used in Ref. [4]. This grid is then used to construct one coarser and two finer grids. The coarser grid, containing 48×18 cells, is constructed by merging together groups of four cells in the original grid. A 192×72 grid is created by cutting each cell of the original grid in four equal parts. Each of the resulting cells in again cut into four equal parts to obtain a 384×144 grid, which far exceeds the resolution that is commonly used in the community. The magnetic field strengths are linearly interpolated for the finer grids, and averaged for the coarse grid. Figure 1 displays the resulting grids.

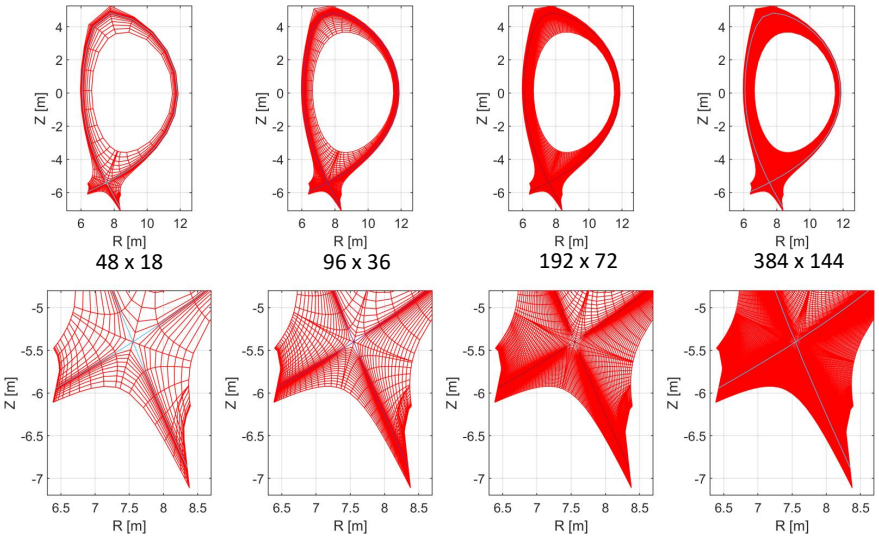

Figure 1: The four different grids used in this study. Full domain (top) and zoom of the divertor (bottom).

3.2. Boundary conditions and anomalous transport

All simulations have a deuterium core ion density of $5 \cdot 10^{19}$ m^{-3}. The multi-species cases have additional core densities of 10^{18} m^{-3} and 10^{15} m^{-3} for the fully stripped helium an argon ions, respectively.

At the radial boundaries, decay lengths of 3 cm are imposed for the densities and temperatures. A recycling factor of 99% is imposed for the deuterium atoms at the private flux boundary.

The five cases differ in their number of species, their core temperatures, and their anomalous transport coefficients. The anomalous transport is defined through the anomalous diffusion coefficient, $D_\mathrm{i}^{(\mathrm{AN})}$, the anomalous viscosity $\eta_\mathrm{i}^{(\mathrm{AN})}$, and the anomalous ion and electron conductivities, $\chi_\mathrm{i}^{(\mathrm{AN})}$ and $\chi_\mathrm{e}^{(\mathrm{AN})}$. Table 1 details the case setups. Case 3 and 5 use a transport profile instead of spatially constant anomalous transport coefficients, as explained in the next section. The profiles are only defined for $D_\mathrm{i}^{(\mathrm{AN})}$, $\chi_\mathrm{i}^{(\mathrm{AN})}$, and $\chi_\mathrm{e}^{(\mathrm{AN})}$. We set $\eta_\mathrm{i}^{(\mathrm{AN})} = 1$ kg m^{-1} s^{-1}.

	Species	Core T_i & T_e	Transport
Case 1	D	1000 eV	$D_\mathrm{i}^{(\mathrm{AN})} = 0.3; \chi_\mathrm{i}^{(\mathrm{AN})} = \chi_\mathrm{e}^{(\mathrm{AN})} = \eta_\mathrm{i}^{(\mathrm{AN})} = 1$
Case 2	D	700 eV	$D_\mathrm{i}^{(\mathrm{AN})} = \chi_\mathrm{i}^{(\mathrm{AN})} = \chi_\mathrm{e}^{(\mathrm{AN})} = \eta_\mathrm{i}^{(\mathrm{AN})} = 1$
Case 3	D	700 eV	Transport profile from Figure 2
Case 4	D + He + Ar	1000 eV	$D_\mathrm{i}^{(\mathrm{AN})} = \chi_\mathrm{i}^{(\mathrm{AN})} = \chi_\mathrm{e}^{(\mathrm{AN})} = \eta_\mathrm{i}^{(\mathrm{AN})} = 1$
Case 5	D + He + Ar	500 eV	Transport profile from Figure 2

Table 1: Case descriptions.

For the multi-species cases, the simulations with the finest grid are still running, so they are not yet discussed in the remainder of the paper. I expect the simulations to be converged before the PET paper deadline.

3.3. Radially dependent transport coefficients

Complex edge phenomena such as H-mode transport barriers, can not yet be simulated self-consistently in codes like SOLPS-ITER. Instead, transport barriers are typically imposed through radially dependent anomalous diffusion coefficients. Here, we use transport profiles based on those used in Ref. [4] for cases 3 and 5. The transport profile is defined through 38 discrete points with a certain radial distance along the outer midplane (OMP). These values are then linearly interpolated to the cell centers along the OMP. The profiles for the different grids, resulting from the linear interpolation, are shown in Figure 2. It can be seen that the linear interpolation causes slight difference between the different grids. The finer grids have several discrete values in the "vertical" parts of the profile, while the coarsest grids has no cells there. This effect is expected to give a contribution to the discretization error.

4. Results

4.1. Outer target and OMP profiles

Figure 3 shows the ion temperature, deuterium ion particle flux, Γ_i, and total heat flux (excluding radiation), Q_t, along the length of the outer target. $\mathrm{s} - \mathrm{s}_\mathrm{sep}$ is constructed as the cumulative sum of the target face lengths, offset by the cumulative sum of target face lengths until the separatrix. The T_i, Γ_i and Q_t values are plotted in the middle of each cell face. Furthermore, we show the electron temperature along the OMP.

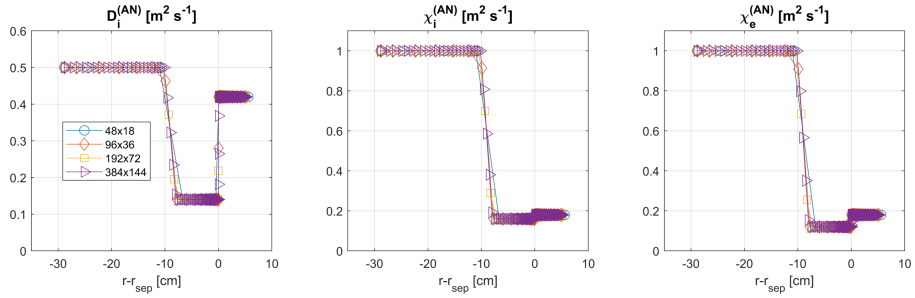

Figure 2: Radially dependent anomalous transport profiles for the four different grids resulting from linear interpolation from the original profile data to the cell centers along the OMP for each grid.

When performing a grid convergence study, some care is needed regarding which values are compared exactly. After all, because we have split each cell in four equal pieces, the cell centers of the different grids do not lie on the same physical coordinate, while Richardson's formula (Eq. 3) requires the values to be defined in the same location. For T_i along the outer target, we take the values in the guard cells, and not the values in the first physical cells, such that the values are defined at identical poloidal coordinates. Γ_i and Q_t are defined on the target cell face, so they are automatically defined at the same poloidal coordinate. For T_e along the OMP, we plot along the radial coordinates $\mathrm{r} - \mathrm{r}_\mathrm{sep}$ of the original grid. For the 192×72 and 384×144, we perform an unweighted average between the four cells which surround the cell centers of the original grid. The coarsest grid is omitted for these plots.

The results on the four grids agree qualitatively, and the results appear to be close to grid convergence, showing only small differences between the finest and second-finest grid. Only for the deuterium ion particle flux, the differences between the three finest grids are more substantial, and the coarsest grid results in a completely erroneous result. This points to strongly non-linear local effects. For Case 2, there are strange "ripples" on the ion temperature profile for the two finest grids. We hypothesize that this is a numerical artifact resulting from the fact that each cell was cut in four equal parts, instead of the grid being smoothly regenerated from scratch.

4.2. Estimation of convergence order and discretization error

Figure 4 displays the estimates of the order of convergence, calculated with Eq. 4, using the three finest grids. The estimate is performed for several quantities of interest: the peak deuterium ion particle flux density (max Γ_i) at the inner and outer target (IT/OT), the peak heat flux (max Q_t) at inner and outer target, and the electron density and temperature at the crossing of the separatrix and the OMP.

We find a very large spread on the estimates for p_d, meaning that these estimates cannot be reliably used to estimate the discretization error. Hence, we take $p_\mathrm{d} = 1$.

Figure 5 displays the estimated discretization errors for the three finest grids. The discretization error on the original grid lies below 25 % for all but one measured quantity of interest. Only the peak deuterium ion flux density at the outer target has a much larger discretization error of 100 %. The 384×144 grid naturally has the lowest discretization error, below 10 % for all but one measured quantity of interest. The maximum Q_t along

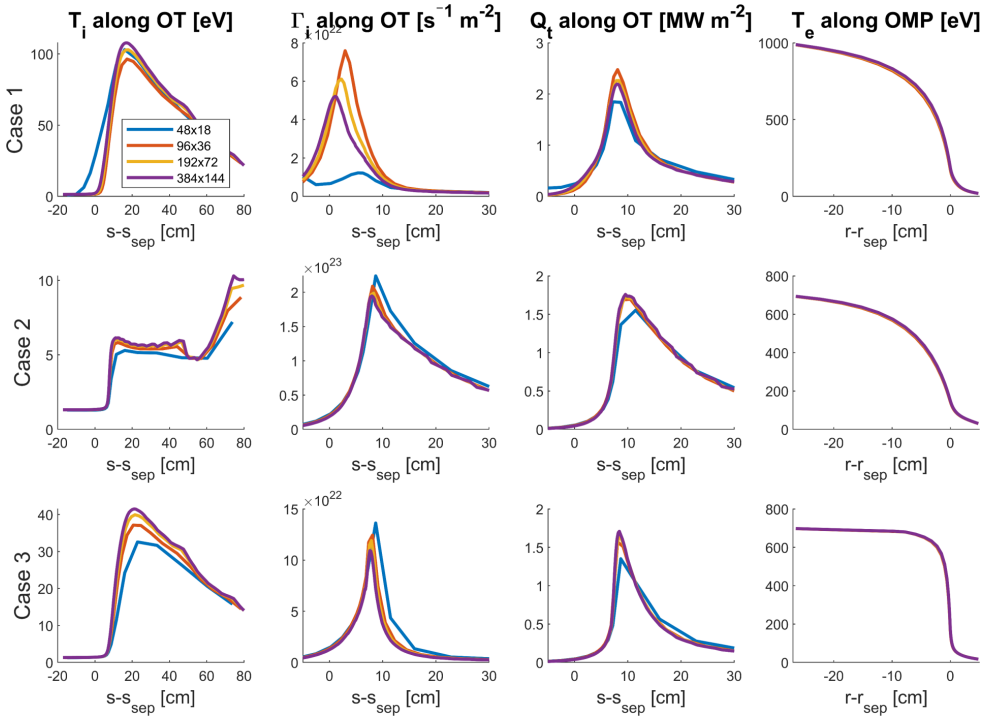

Figure 3: Ion temperature (left) and total heat flux density (middle) along the outer target plate, and electron temperature along the OMP (right), for the four different grids.

the outer targets is one of the most important outputs of a plasma boundary simulation. For this quantity, the case-averaged discretization error is 13.7 % for the original grid, 7.5 % for the 192×72 grid, and 4 % for the 384×144 grid.

4.3. Computational requirements

At present, the B2.5 code employs a direct matrix solver and is not parallelized. This leads to a very poor scaling in computational walltime with increasing mesh size. The simulations are performed on Xeon Gold 6140 CPUs@2.3 GHz (Skylake) processors at the Flemish Supercomputer Centre (VSC). Table 2 lists the average computational time per timestep for the D-only and multispecies cases, for each grid. The total simulation time for each case is then found by multiplying with the number of timesteps needed to arrive a the required convergence criterion. This varies strongly depending on the case (boundary conditions, regime, number of species, intitial state, etc). The total number of timesteps was not tracked by the author, but 5000-50000 are typical numbers.

5. Conclusions and future work

The choice of grid resolution for plasma boundary simulations remains a difficult trade-off between numerical accuracy and computational time. The discretization error on the

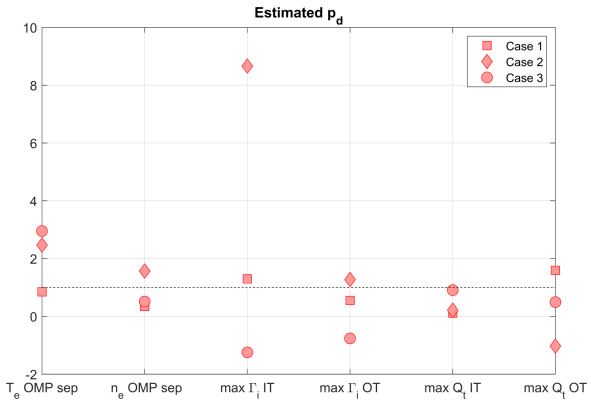

Figure 4: Estimated convergence orders for different quantities of intrest, for the three D-only cases.

	#species	48×18	96×36	192×72	384×144
D-only	2	0.52 s	3.44 s	22.05 s	166.15 s
D + He + Ar	24	3.38 s	25.2 s	129.45 s	648 s

Table 2: Average CPU time per timestep

original 96×36 grid was found to be mostly in the 4-25 % range, with an exception of 100 % for the peak deuterium particle flux density on the outer target. The discretization error approximately halves when refining the grid by a factor of 2, although we showed that this scaling is not followed exactly, presumably due to the many non-linear terms encountered in plasma boundary simulations. Refining the grid, however, significantly increases the computational cost. Further coarsening of the original grid led to completely erroneous solutions for some cases, hence the use of such grids is discouraged. We showed that the discretization error is highly case dependent, and hence it is not possible to give a definitive advice on which resolution should be used for future DEMO studies. A possible solution is to use the original 96×36 grid for large parameter scans, but to use a more refined grid for a subset of the cases.

It could investigated if the B2.5 code can be sped up through parallelism. This is especially true when coupling with an MPI-parallelized EIRENE version, because then multiple cores are being reserved for the duration of the full run anyway.

Regarding future work, the presented study should extended by studying more realistic high power cases and using kinetic instead of fluid neutrals.

6. Acknowledgements

The first author is funded by a PhD fellowship of the Research Foundation - Flanders. Parts of this work have been carried out within the framework of the EUROfusion Consortium, funded by the European Union via the Euratom Research and Training Programme (Grant Agreement No 101052200 — EUROfusion). Views and opinions expressed are however those of the author(s) only and do not necessarily reflect those of

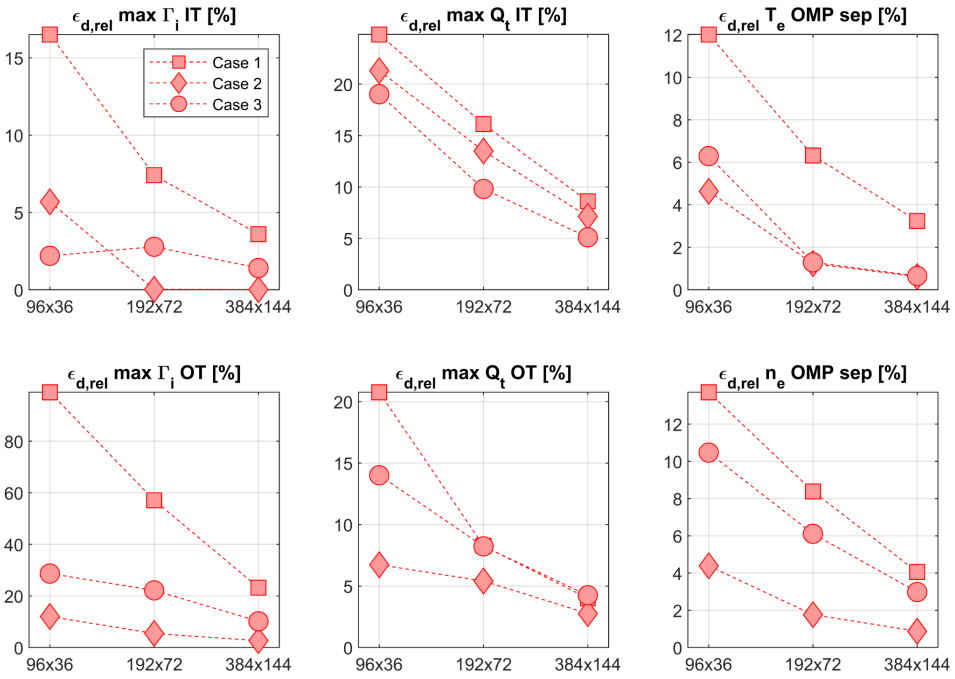

Figure 5: Estimated discretization errors for the three finest grids for the three D-only cases.

the European Union or the European Commission. Neither the European Union nor the European Commission can be held responsible for them. The computational resources and services used in this work were provided by the VSC (Flemish Supercomputer Center), funded by the Research Foundation Flanders (FWO) and the Flemish Government - department EWI.

References

[1] S. Wiesen, D. Reiter, V. Kotov, M. Baelmans, W. Dekeyser, A. Kukushkin, S. Lisgo, R. Pitts, V. Rozhansky, G. Saibene, et al., The new SOLPS-ITER code package, Journal of Nuclear Materials 463 (2015) 480–484.

[2] X. Bonnin, W. Dekeyser, R. Pitts, D. Coster, S. Voskoboynikov, S. Wiesen, Presentation of the new solps-iter code package for tokamak plasma edge modelling, Plasma and Fusion Research 11 (2016) 1403102–1403102.

[3] A. Kukushkin, H. Pacher, V. Kotov, G. Pacher, D. Reiter, Finalizing the iter divertor design: The key role of solps modeling, Fusion engineering and design 86 (12) (2011) 2865–2873.

[4] F. Subba, D. Coster, M. Moscheni, M. Siccinio, Solps-iter modeling of divertor scenarios for eu-demo, Nuclear Fusion 61 (10) (2021) 106013.

[5] V. Korzueva, E. Kaveeva, E. O. Vekshina, V. A. Rozhansky, I. Y. Senichenkov, A. Shirobokov, D. P. Coster, Solps-iter modeling of eu-demo ar-seeded cases with drifts and kinetic neutrals, Plasma Physics and Controlled Fusion.

[6] E. Vekshina, V. Korzueva, V. Rozhansky, I. Senichenkov, E. Kaveeva, I. Veselova, D. Coster, F. Subba, Solps-iter eu-demo modelling with drifts and kinetic neutrals, Contributions to Plasma Physics 62 (5-6) (2022) e202100176.

[7] S. Braginskii, M. Leontovich, Reviews of plasma physics (1965).

[8] D. Reiter, M. Baelmans, P. Börner, The EIRENE and B2-EIRENE codes, Fusion Science and Technology 47 (2) (2005) 172–186.
[9] K. Ghoos, P. Börner, W. Dekeyser, A. Kukushkin, M. Baelmans, Grid resolution study for b2-eirene simulation of partially detached iter divertor plasma, Nuclear Fusion 59 (2) (2018) 026001.
[10] P. J. Roache, Perspective: a method for uniform reporting of grid refinement studies.
[11] D. Boeyaert, S. Carli, K. Ghoos, W. Dekeyser, S. Wiesen, M. Baelmans, Numerical error analysis of solps-iter simulations of east, Nuclear Fusion 63 (1) (2022) 016005.
[12] P. J. Roache, et al., Conservatism of the grid convergence index in finite volume computations on steady-state fluid flow and heat transfer.
[13] N. Horsten, G. Samaey, M. Baelmans, Development and assessment of 2D fluid neutral models that include atomic databases and a microscopic reflection model, Nuclear Fusion 57 (11) (2017) 116043.
[14] W. Van Uytven, W. Dekeyser, M. Blommaert, N. Horsten, Y. Marandet, M. Baelmans, Advanced spatially hybrid fluid-kinetic modelling of plasma-edge neutrals and application to ITER case using SOLPS-ITER, Contributions to Plasma Physics (2022) e202100191.
[15] W. Dekeyser, P. Börner, S. Voskoboynikov, V. Rozhanksy, I. Senichenkov, E. Kaveeva, I. Veselova, E. Vekshina, X. Bonnin, R. Pitts, et al., Plasma edge simulations including realistic wall geometry with SOLPS-ITER, Nuclear Materials and Energy 27 (2021) 100999.
[16] R. Schneider, X. Bonnin, K. Borrass, D. Coster, H. Kastelewicz, D. Reiter, V. Rozhansky, B. Braams, Plasma edge physics with B2-EIRENE, Contributions to Plasma Physics 46 (1-2) (2006) 3–191.